Imran ALI and İsmail Hakkı KARA

THE HOT ROLLING SPEED ON MICROSTRUCTURE, MACROTEXTURE AND MECHANICAL PROPERTIES OF MG-2.5AL-1.0SN-0.3MN-0.4LA-0.16GD MG ALLOY

KEYWORDS

Keywords: Mg-2.5Al-1.0Sn-0.3Mn-0.4La-0.16Gd, Tensile test, hot rolling.

ABSTRACT

This study aims to search for microstructure and tensile properties (at 25°C), of Mg-2.5Al-1.0Sn-0.3Mn-0.4La-0.16Gd Mg alloy produced by low pressure die casting method. The hot rolling process was exposed to the produced alloy at different three speeds of 1.5, 4.7, and 10 m/min. The increased hot rolling speeds resulted in decreased average grain size, twins fraction, and hardness Brinell but the increased DRXs formation. The rising of hot rolling speeds enabled the rising YS, UTS, and elongation % values. The fragmentation of secondary phases including La and Gd demonstrated homogeneously distribution inside the matrix phase of the specimen hot-rolled at 10 m/min which enhanced the room temperature tensile properties. The intergranular and secondary phases introduced cracking formed in the hot-rolled specimens at lower and higher speeds, respectively.

1. Introduction

Magnesium (Mg) alloys have been practised by the automotive industry to diminish the emission and develop the energy efficiency because of their low density. However, the moderate mechanical properties give rise to alternative material choosing to automotive producers such as alumınum alloys. On the other hand, the rare earth metals (REMs) have been used to enhance the mechanical properties of Mg alloys and notable results have been achieved. Last years the Mg-Al-Sn ternary alloy system has been attracting incredible attention by researchers due to the Sn enables excellent properties such as high stretch formability, superior creep resistance and high temperature tensile strengths. Wang Ji. and et.al developed a new Mg–Al–Sn–RE sheet with high ductility at room temperature using Y and Nd as REMs, where the YS and UTS values were obtained as 168 and 257 MPa, respectively [1]. Mg-xAl-ySn-0.3Mn magnesium alloys were designed by She J. and et.al. They reported gradual increasing in yield strength and yield-to-tensile strength ratio was obtained by suppression of DRX in Mg–xAl–ySn–0.3Mn (x = y = 1, 3) alloys with decreasing Al content or extrusion temperature [2].

Lanthanum (La) is a known low cost light rare earth metal and is a candidate to develop new Mg alloys. It is very useful to protect the Mg alloys in corrosive environments when the amount of La is less than 0.7%wt [3]. Moreover, minor La addition to Mg alloys also results in promising mechanical properties [4]. Furthermore, Song Y. and et. al. investigated the amount of La in the range of 0.2–0.8%wt. on the discharge behavior of Mg alloy, where it is found that 0.4La %wt. indicated the most negative discharge potential [5].

Gadolinium (Gd) has the high solid solubility (23.49 wt%) capability in Mg at 548 °C [6], , but reducing is seen as 3.82 wt% at 200 °C, thus the aging response of Gd is very high [7]. GdMgSn phase formation was discovered in the Mg–3Sn–2Ca alloy by Yang M. and et.al and the amount of GdMgSn phase increased when the rising Gd amounts from 0.42 wt.% to 1.79 wt.% [8]. Al2Gd phase was introduced in the produced AZ91 by Huisheng C. and et. al. They found that the amount and size of the Al2Gd phase increased with the increasing Gd amount [9]. Song Y. and et.al. obtained that the addition of Gd promotes the formation of Al2Gd, effectively reducing the volume fraction of the β-Mg17Al12 phase [10].

The hot rolling process including temperature, strain rate, rolling speed and deformation rate per pass parameters is utilized to obtain sheet Mg alloys displaying fine grains. Mg-2.5Nd-0.5Zn-0.5Zr alloy sheet was prepared by the high strain rate rolling (HSRR) at different temperatures of 623 K, 648 K and 673 K with strain rate $\dot{\varepsilon}$ was 6.17 s−1. The HSRR resulted in finer and

homogeneously distributed microstructure which include percentage of recrystallization were 46.1%, 49.3% and 63.9% for hot rolled specimens at 623 K, 648 K and 673 K, respectively [11]. Different amounts of rolling deformations (40%, 60% and 80%) were applied to Mg–1Al–4Y alloy and the rising deformation amount decreased the grain size. Moreover, fracturing of coarse grains was observed by the increasing rolling deformation. further, the secondary phases uniformly placed on the grain boundaries and in the grains as well as became smaller when high deformation rates were applied [12]. Similarly, the effect of rolling speed imparts uniform microstructure and rising of recrystallization degree [13].

It is reported that Mg-Al-Sn alloys were capable of excellent microstructure [14], corrosion [15] and texture properties [1]. However, the effect of both La and Gd on the microstructure, mechanical properties of Mg-Al-Sn alloys still needs attention due to the response of secondary phase containing La and Gd to the changed hot rolling speeds. This study aimed to investigate the effect of hot rolling speeds on the microstructure, room temperature mechanical properties of Mg-2.5Al-1.0Sn-0.3Mn-0.4La-0.16Gd alloy.

2. Experimental Studies

Materials were produced using the low-pressure permanent mold casting technique. Pure Mg, pure Al and pure Sn were first added to the crucible. The casting temperature was determined as 750°C degrees and it waited for 1 hour for the pure metals to melt. Afterwards, master Mg-La, Mg-Gd and Mg-Mn were added. The molten materials were mixed during the waiting period of 15 minutes. Pure argon gas was continuously supplied throughout the melting process. The transfer of molten metals to the stainless steel mold was carried out under 2–3 atm pressure. The chemical composition of the produced material that was determined by X-ray fluorescence spectrometer device (Rigaku Primus II-WD-XRF) consists of Mg-2.5wt%Al-1.0wt%Sn-0.3wt%Mn-0.4wt%La-0.16wt%Gd Slab materials of 36X36X12 mm were converted into sheet materials with a thickness of 2 mm. The conventional rolling process was used for this process by using a hot rolling machine (Yılmaz Makine Sanayi/Turkey) with a diameter of 110 mm rollers. Before hot rolling, the slabs were kept at 350°C degrees for 30 minutes and the rolling was completed at the same temperature. In a total of 8 passes, approximately 83% of the materials were deformed. Waited 5 minutes at 350°C degrees between passes. The sheet materials were cooled in water. Hot rolling parameters include 20% deformation rate per pass and three different rolling speeds of 1.5,4.7 and 10 m/min. The abbreviation of A1, A2 and A3 is determined for 1.5,4.7 and 10 m/min speed rolling specimens, respectively. Grinding (400–2500 grids), polishing (1um) and etching (70ml ethanol-10ml pure water-10ml acetic acid-4.2 gr picric acid) processes were carried out to examine the microstructure of sheet materials, respectively. The twinning and grains were revealed by the light optical microscopy (LOM) technique. The shape and distribution of the secondary phases were investigated with a scanning electron microscope (Carl Zeiss ULTRA PLUS FE-SEM). The type of secondary phases was determined by X-ray Diffraction (XRD-Machine: RIGAKU Ultima IV) method. Moreover, the particle size of secondary phases was calculated from multiple SEM images, where a linear intercept method was used. Twins fraction was obtained by average five to seven LOM images were taken of each sample at magnification ranging from 100X-200X according to ASTM E562-02.The types of secondary phases were investigated by the XRD method. Moreover, X-ray diffractometer (Rigaku ULTIMA IV) was used for secondary phase characterization. Three pole figures {0002}were used to calculate the orientation distribution function (ODF) using the MATLAB toolbox MTEX software. The universal Brinell hardness test vehicle (Bulut Machine Industry Hardness Test) was employed at 187.5 kg load with 2.5 mm ball diameter during 10 seconds. Tensile tests were conducted with a universal testing machine (Zwick/Roell Z600) at room temperature with a 2 mm/min test speed. Fracture surfaces of tensile specimens were analyzed by SEM-EDS (EDS, Quantax 200, Bruker) to clarify which mechanism plays a role during breaking.

3. Results

3.1. Microstructure

3.1.1. LOM and SEM

Fig. 1 shows the LOM micrographs consisting of A1, A2, and A3 specimens. The equiaxed grains after hot rolling deformation were placed on the

microstructure of all investigated specimens. However, the difference is characterized by the formation density of twins and the dynamically recrystallized grains depend on the rolling speed. The specimens include non-homogeneous sized grains and some of them are untwinned. DRX formation is achieved by the rising of hot rolling speed. The average grain size calculation shows that the high rolling speed results in high DRXs formation. However, the twins fraction value is as the ascending order A1>A2>A3 (see Table 1).

Table 1. Hardness Brinell, average grain size and twins fraction of A1, A2 and A3 specimens

Specimen	Hardness (HBW)		Average grain size (μm)		Twins Fraction	
A1	68.18	±1.68	25.65	±4.6	0.42	±0.002
A2	67.9	±0.48	17.07	±0.75	0.19	±0.075
A3	60.58	±1.08	16.03	±0.45	0.13	±0.005

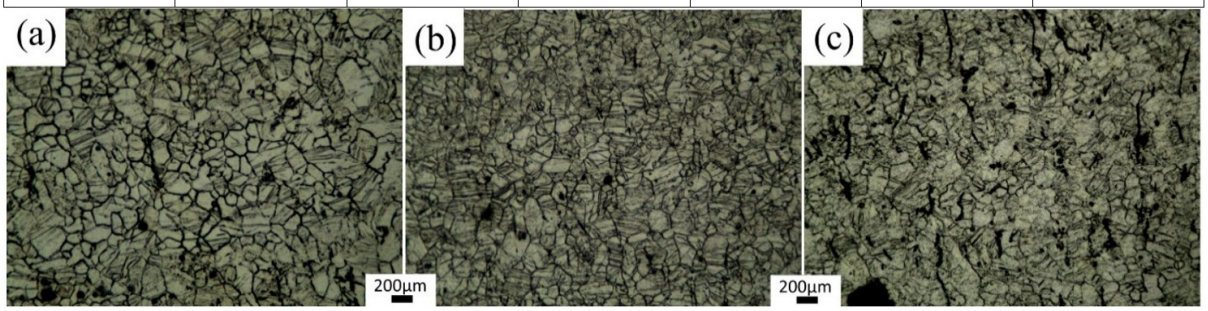

Fig. 1. Optical microscopy of A1, A2, and A3

Fig.2 illustrates the SEM micrographs of A1, A2, and A3 specimens. Secondary phase distribution and types are different for the investigated sample. Because as seen Fig. 2a and Table 2, the globular and acicular type-shaped secondary phases consist of Al-La and Mg-Gd rich composition. Secondary phase formation of A1 specimens is mostly observed on the grain boundaries. However, the rising of hot rolling speed resulted in fragmentation of secondary phases which were located inside of grains. Further, the Al-Mn-Gd rich globular type secondary phases amount decreased as it is seen Fig. 2b. Because most secondary phases are broken to Al-La-Gd rich particles that were accommodated on the grain boundaries. Moreover, the A3 specimen includes the highest density of fine-scaled secondary phases that were predominantly placed inside of grains. It can be said that the highest hot rolling speed is beneficial for distributing the fine-scaled secondary phases.

Table 2. The EDS results was obtained A1,A2 and A3 specimens

Points in Fig.2	Mg	Al	Mn	Sn	La	Gd
Fig.2a Point 1	8.88	36.35	2.17	0.23	44.35	8.01
Fig.2a Point 2	70.28	2.31	0.17	0.84	0.00	29.41
Fig.2b Point 1	3.37	34.29	40.98	0.00	3.48	27.60
Fig.2b Point 2	18.27	29.90	2.03	0.00	37.28	12.51
Fig.2c Point 1	62.62	21.95	0.00	7.35	0.00	8.08
Fig.2c Point 2	49.75	8.48	2.70	0.05	15.97	23.05

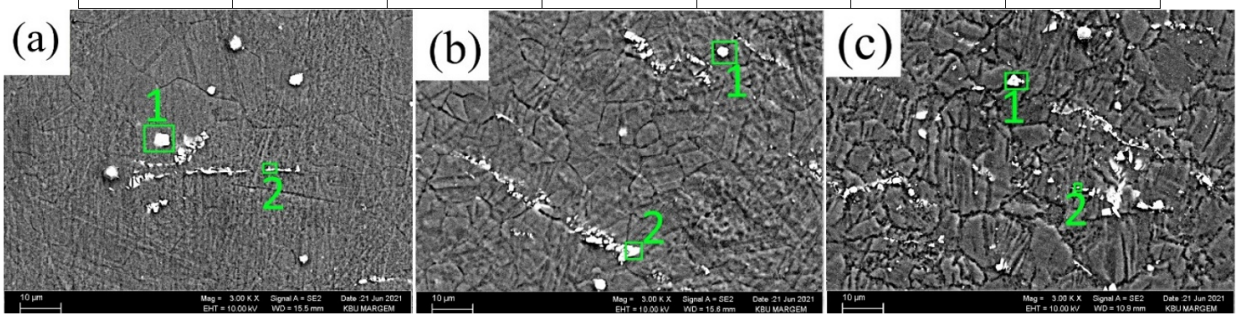

Fig. 2. Scanning Electron Microscopy of A1, A2, and A3

3.1.2. XRD and Pole Figure

The Fig. 3 presents the XRD pattern of A1, A2, and A3 specimens. Mg_2Sn, $Al_2(Gd, La)$ and $Mg_5(Gd, La)$ were detected at 22.52°, 20.36° and 28.86° as a secondary phase, respectively.

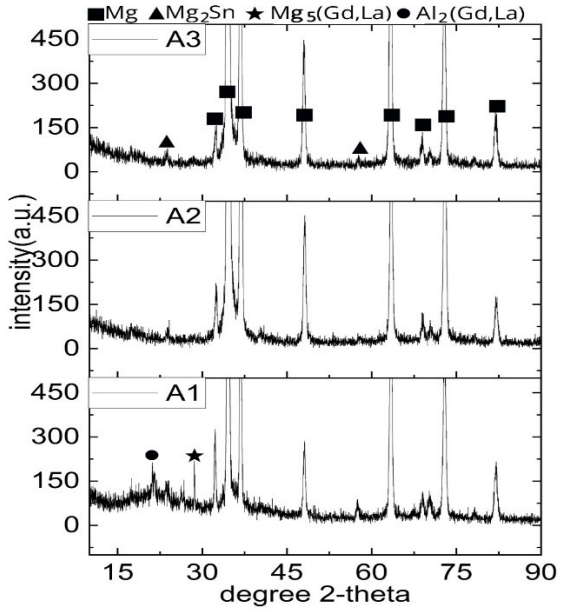

Fig. 3. XRD patterns for A1, A2, and A3

Pole figure measurement is given in Fig. 4. The (0002) basal plane intensity values show that the highest one was measured by the specimen of A2 which is followed in descending order A3 and A1. A typical strong basal pole in the A2 specimen was observed around the ND direction. However, the tilting of the basal pole through the TD direction was observed by A1 specimen. Moreover, the spread in the basal pole towards 45 degrees between RD and TD was obtained by the specimen of A3.

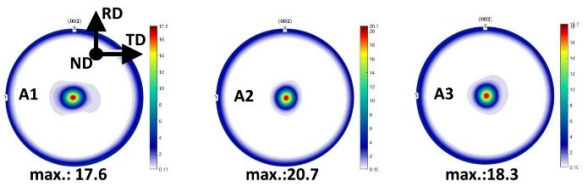

Fig. 4. Pole figure measurement of A1, A2, and A3

3.2. Hardness Properties

The hardness brinell was utilized to measure the combined effect of grain, twins, and secondary phase boundaries on the hardness properties of investigated specimens. It is seen that the hardness is influenced by the hot rolling speed, where the lower hardness was measured with the increasing

rolling speed (see Table 1). The DRXs are known as dislocation-free grains, enabling soft structure [16] and [17].

3.3. Tensile Test Results at Room Temperature

The stress-strain curves belonging to A1, A2, and A3 specimens are presented in Fig. 5 as well as the tensile test results given in Table 3. It is seen that the hot rolling speed results in high performance about the YS, UTS, and elongation % properties. The microstructure of investigated specimens proved that the high rolling speed imparts to finer scaled secondary phases which are mostly distributed inside of the grains due to the applied high deformation energy during high speed rolling. It is reported by Yu.D and et. al. that the high density of fine-scaled secondary phases under ~100 nm size restricts the growth of DRXs during hot deformation [18]. Moreover, the DRXs enable random orientations thus they weaken the strong fiber texture of Mg alloys [19]. It is confirmed by the average grain size calculation that it is ordered as A1 > A2 > A3. However, the twins also influence the texture of Mg alloys. It is said that regulation of Mg microstructure by twins can be accomplished with the grain refinement thanks to the subdivision of twin boundaries, and changes in crystal lattice orientation, where the {10–12} twins by way of precompression encourage a new grain structure consisting of low internal strain energy and a dual ND- and RD-oriented texture [20]. This change allows higher compressive YS values to AZ31 Mg alloys [21]. The texture intensity of A1 is diminished by the higher twins fraction and then rising rolling speeds eliminated the twins due to enhancing the formation of DRXs, where texture is increased. However, the homogeneously distributed fine-scaled secondary phases of the A3 specimen result in decreasing texture when we compare it with A2. Cracked secondary phases are useful to the developed ductility, as a result of diminished stress concentration and preventing premature failure [22] and [23].

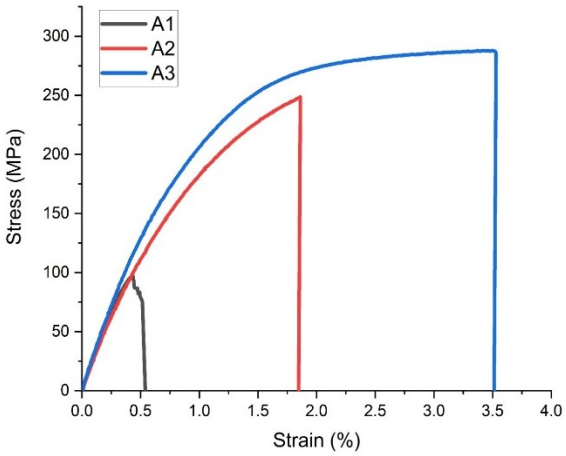

Fig. 5.

3.4. Fractured Surface of Tensile Specimens

Fig. 6 illustrates the fracture surface of A1, A2, and A3 specimens. We can say that generally known as cleavage-type brittle fracture occurred on all specimens, specific to polycrystalline materials. In SEM images, we can distinguish cleavage-type refractions from glossy and reflective surfaces. The cleavage-fracture pattern contains an image lined up in layers extending like a river. The rolling speed affects the cleavage width. The fine layers mostly appeared by the increasing rolling speed. Moreover, fine-scaled secondary phase particles were observed in the layers of A1 and A3 specimens. However, the larger ones are mostly placed on the fractured surface of A2. The rupture during tensile tests started on the grain boundaries of A1 and A2 specimens, which shows the intergranular cracking. However, the fracture of the A3 specimen is enlarged through the secondary phase located areas (see Fig. 7).

Table 3. Room temperature tensile properties of A1, A2 and A3 specimens

Specimen	UTS (MPa)	YS (MPa)	Strain (mm/mm)
A1	96.9±2.1	82.220±1.9	0.436±0.01
A2	248.7±3.4	158.319±2.1	1.861±0.06
A3	287.9±3.9	174.985±3.1	3.498±0.11

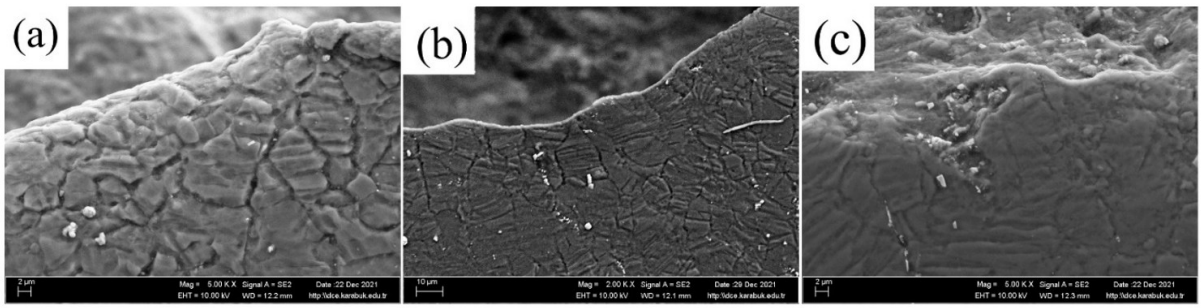

Fig. 6. Fracture surface for A1, A2, and A3

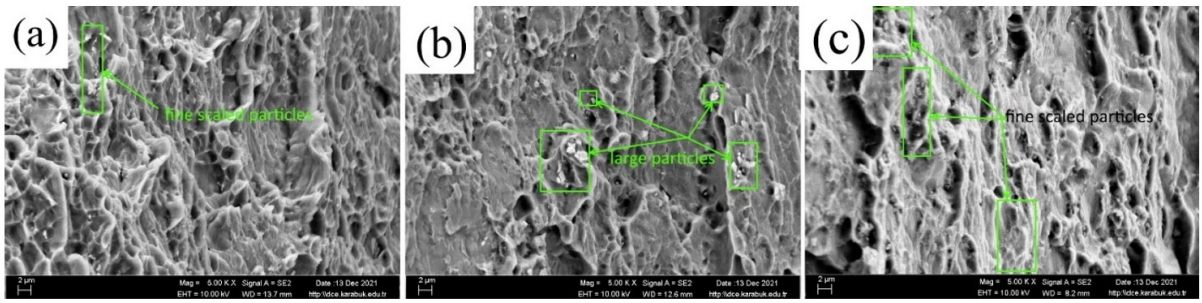

Fig. 7. Fracture surface for A1, A2, and A3

Conclusions

The obtained results can be summarized as follows;

1. The application of different hot rolling speeds on Mg-2.5Al-1.0Sn-0.3Mn-0.4La-0.16Gd Mg alloy resulted in diverse microstructure properties such as twins dominated and DRXs dominated for applied 1.5 m/min and 29.5 m/min hot rolling speeds, respectively.
2. The room temperature tensile properties prove that the fine-scaled secondary phases obtained by the increased hot rolling speed (29.5 m/min) result in the highest YS, UTS, and elongation % values. The increasing applied hot rolling speed enables the increasing YS, UTS, and elongation % value.

Funding

This work was financially supported by the Scientific Research Projects Coordination Unit of Karabük University, Project Number: KBÜBAP-21-YL-086

References

1. J. Wang, X. Zhang, Y. Yang ve Z. Wang, Microstructure, texture and mechanical properties of hot-rolled Mg–4Al–2Sn–0.5Y–0.4Nd alloy, *J. Magnes. Alloys,* 2016,4 (3), pp. 207–213.

[2] J. She, F. Pan, J. Zhang, A. Tang, S. Luo ve Z. Yu, Microstructure and mechanical properties of Mg–Al–Sn extruded alloys, *J. Alloys Compd.,* 2016, 657, p. 893-905.

[3] A. Prasad, Y. Chiu, S. Singh, N. Gosvami ve J. Jain, Role of La addition for enhancing the corrosion resistance of Mg–Dy alloy, *Corros. Eng. Sci. Technol.,* 2021, 56(6), pp. 575–583.

[4] A. Prasad, S. Si, U. Ghori, S. Thirunavukkarasu, Y. Chiu, I. Jones, S. Lee, S. Singh, N. Gosvami ve J. Jain, Effect of La addition on precipitation hardening in Mg–10Dy alloy, *Mater.,* 2020, 14, p. 100898.

[5] Y. Song, H. Yang, Y. Chai, Q. Wang, B. Jiang, L. Wu, Q. Zou, G. Huang, F. Pan ve A. Atrens, Corrosion and discharge behavior of Mg–xLa alloys (x=0.0–0.8) as anode materials, *Trans. Nonferrous Met. Soc. China,* 2021, 31 (7), p. 1979–1992.

[6] H. Okamoto, Gd-Mg (Gadolinium-Magnesium), *Journal of Phase Equilibria,* 1993, 14, p. 534–535.

[7] K. Liu, F. Lou, Z. Yu, Z. Wang, S. Li, X. Du ve W. Du, Microstructures and mechanical properties of Mg-6Gd-1Er-0.5Zr alloy sheets produced with different rolling temperatures, *J. Alloys Compd.,* 2022, 893, p. 162213.

[8] M. Yang, Y. Zhu, X. Liang ve F. Pan, Effects of Gd addition on as-cast microstructure and mechanical properties of Mg–3Sn–2Ca magnesium alloy, *Mater. Sci. Eng. A,* 2011, 528(3), p. 1721–1726.

[9] H. Cai, F. Guo, J. Su ve L. Liu, Existing forms of Gd in AZ91 magnesium alloy and its effects on mechanical properties, *Mater. Res. Express,* 2019, 6, p. 066541.

[10] Y. Song, Q. Liu, H. Wang ve X. Zhu, Effect of Gd on microstructure and stress corrosion cracking of the AZ91-extruded magnesium alloy, *Corros. Mater,* 2021, 72, p. 1189-1200.

[11] S. Wang, W. Zhang, H. Wang, J. Yang, W. Chen, G. Cui ve G. Wang, Microstructures evolution, texture characteristics and mechanical properties of Mg-2.5Nd-0.5Zn-0.5Zr alloy during the high strain rate hot-rolling, *Mater. Sci. Eng. A,* 2021,803, p. 140488.

[12] J. Wang, P. Jin, X. Li, F. Wei, B. Shi, X. Ding ve M. Zhang, Effect of rolling with different amounts of deformation on microstructure and mechanical properties of the Mg–1Al–4Y alloy, *Mater. Charact.,* 2020, 161, p. 110149.

[13] W. Jia, Y. Tang, F. Ning, Q. Le ve L. Bao, Optimum rolling speed and relevant temperature- and reduction-dependent interfacial friction behavior during the break-down rolling of AZ31B alloy, *J. Mater. Sci. Technol.,* 2018, 34, pp. 2051–2062.

[14] A. S. H. Kabir, M. Sanjari, J. Su, I.-H. Jung ve S. Yue, Effect of strain-induced precipitation on dynamic recrystallization in Mg–Al–Sn alloys, *Mater. Sci. Eng. A.,* 2014, 616, pp. 252–259.

[15] Z. Yu, Q. Huang, W. Zhang, C. Luo, H. Guan, Y. Chen, H. Song, Z. Hu ve C. Luc, Effect of Sn content on the mechanical properties and corrosion behavior of Mg-3Al-xSn alloys, *Mater. Res. Express,* 2020, 7(7), p. 076505.

[16] M. Sabbaghian, R. Mahmudi ve K. Shin, Microstructure, texture, mechanical properties and biodegradability of extruded Mg–4Zn–xMn alloys, *Mater. Sci. Eng. A,* 2020, 792, p. 139828.

[17] L. Chen, J. Zhang, J. Tang, G. Chen, G. Zhao ve C. Zhang, Microstructure and texture evolution during porthole die extrusion of Mg-Al-Zn alloy, *J. Mater. Process. Technol.,* 2018, 259, p. 346-352.

[18] D. Yu, D. Zhang, J. Sun, Y. Luo, J. Xu, H. Zhang ve F. Pan, Improving mechanical properties of ZM61 magnesium alloy by aging before extrusion, *J. Alloys Compd.,* 2017,690, pp. 553–560.

[19] H. Pan, G. Qin, M. Xu, H. Fu, Y. Ren, F. Pan, Z. Gao, C. Zhao, Q. Yang, J. She ve B. Song, Enhancing mechanical properties of Mg–Sn alloys by combining addition of Ca and Zn, *Materials & Design,* 2015, 83, pp. 736–744.

[20] J. Lee , Y. Kim , S. Kim , J. Lee, , M. Kim, S. Choi, B. Moon, Y. Kim ve S. Park, Texture tailoring and bendability improvement of rolled AZ31 alloy using {10–12} twinning: The effect of precompression levels, *J. Magnes. Alloy.,* 2019, 7, pp. 648–660.

[21] S. Xu, T. Liu, H. Chen, Z. Miao, Z. Zhang ve W. Zeng, Reducing the tension–compression yield asymmetry in a hot-rolled Mg–3Al–1Zn alloy via multidirectional pre-compression, *Mater. Sci. Eng. A,* 2013, 565, pp. 96–101.

[22] L. Tong, J. Chu, W. Sun, Z. Jiang, D. Zou, S. Liu, S. Kamado ve M. Zheng, Development of a high-strength Mg alloy with superior ductility through a unique texture modification from equal channel angular pressing, J.*Magnes. Alloy.,* 2021, 9, pp. 1007–1018.

[23] 3. BİLSEL INTERNATIONAL AHLAT SCIENTIFIC RESEARCHES CONGRESS, 08/09 JUNE, 2024.